Mechanical properties of TiN-TiC mixed crystal films

1998 J. Phys.: Condens. Matter 10 111

(http://iopscience.iop.org/0953-8984/10/1/013)

J. Phys.: Condens. Matter **10** (1998) 111–121. Printed in the UK PII: S0953-8984(98)85237-5

Mechanical properties of TiN–TiC mixed crystal films

H Hyakutake, Y Imada, F Honda and K Nakajima

Toyota Technological Institute, 2-12, Hisakata, Tempaku-ku, Nagoya, Japan

Received 20 June 1997, in final form 21 August 1997

Abstract. Deposited films of TiN–TiC systems with solid solutions were prepared over the range 0.2–0.8 in x defined by TiC_xN_{1-x}, using a RF magnetron sputtering method. Tribological properties of the samples were examined as a function of x. Microhardness increased with x, and reached maximum at around 0.7. Adhesive force between the deposited film and the substrate (high-speed steel) were measured by a scratch test. It was obtained that the adhesive force increased with x and reached maximum at about 0.5. The friction coefficient decreased monotonously with x, but showed a tendency to become minimum at 0.4–0.5. The wear rate showed a complex phenomena with the x-value, indicating two maximums at about 0.2 and 0.8.

X-ray diffraction analyses were conducted with the film samples. The change in microhardness with x was clearly associated with the physical breadth. It was found that the major part of physical breadth was due to lattice distortion in all samples. The decrease in $I(111)/I(200)$ also related to the increase in the microhardness. Stacking faults were found to form in the film during the sputtering deposition, suggesting that vacancy platelets were generated in the sample depending on the value of the stacking probability.

1. Introduction

Because of their various useful properties as film TiN and TiC are widely used as materials in industrial applications such as tribological (Ramalingam and Winer 1980, Jamal *et al* 1980), electrical conductive (Wittmer 1985), protective and decorative coatings. It is well known that TiN and TiC form an all-soluble solid solution with a face-centred cubic NaCl structure; the unit cell consists ideally of four atoms of Ti and four atoms of $(N+C)$ atoms. Titanium carbonitride has an excellent hardness and abrasive wear resistance compared with those of each component and has a better chemical stability (Bertoncello *et al* 1992, Tamura *et al* 1994). In fact, TiCN film exhibits high hardness with an average value of 2700 kgf mm^{-2} and good adherence to steel (Narasimhan *et al* 1995).

Tribological and electrical conductive properties of complex ceramic films coated by TiN and TiC should reflect the chemical composition of the film and the defect structure generated during the deposition of both materials. However, little observation has been reported on this point of view.

Hence, the present study was conducted on the change in mechanical properties of the films, especially concerning the tribological properties as a function of adding TiC to TiN by using a RF magnetron sputtering technique.

0953-8984/98/010111+11$19.50

2. Experimental procedure

2.1. Sample preparation

SKD11, which is the equivalent of AISI 'D2', containing 1.5% C, 11% Cr, 1% Mo, etc, $20 \times 10 \times 4$ mm in size, was used as the substrate for film coating. The substrate materials were polished by an emery paper (#1500) at a wet condition, then by buffing, and cleaned with acetone in an ultrasonic cleaner prior to the deposition procedure. The hardness of the substrate was observed at 320 kgf mm^{-2} (3136 MP), and the final stage of the surface roughness was 0.3 μm in R(max). Balls made by SUJ2 (high carbon chromium bearing steel containing 1% C, 0.5% Mn, 1.5% Cr, etc) with R_{max} : 0.4 μm were used as the slider material measuring 4.76 mm in diameter.

TiC_xN_{1-x} films with various values of x were grown by RF magnetron sputtering of complex target of specially made TiN and TiC, in a mixture of argon. x denotes the atomic concentration ratio of carbon defined by $C/(C+N)$ in the TiN–TiC system examined. The target used in the present study is shown schematically in figure 1; it is 10 cm in diameter and 5 mm in thickness. Seven substrates were placed on a line parallel to the boundary line AB on the target shown in figure 1. The geometrical conditions between the target and substrate are also illustrated in this figure.

2.2. Sputtering condition

The base pressure of the system was usually maintained at 5×10^{-5} Pa. High purity argon of 99.999% was used as the sputtering gas. RF etching of the substrate was done

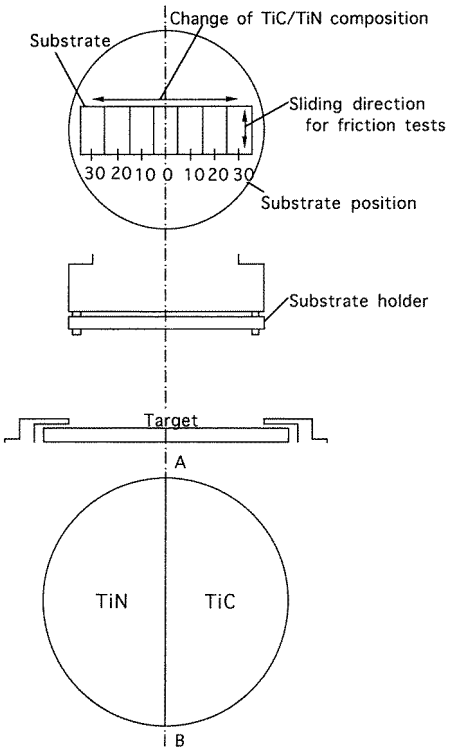

Figure 1. Schematic representation of the substrate position and the target for sputtering.

for 15 min with Ar at a RF power of 100 W under a pressure of 5×10^{-2} Pa. The target-to-substrate distance of 50 mm was maintained throughout the experiment. The total chamber pressure during the sputtering process was 7×10^{-1} Pa and the net RF power was 300 W. The thickness of individual films was estimated from the change in weight of the substrate before and after sputter deposition using an analytical electronic balance (accuracy of 10 μg). Scanning electron microscopic observation on the fracture section of the samples was sometimes done as another method of measuring the film thickness. The temperature of the substrate before and after deposition was observed to be about room temperature and approximately 120 °C, respectively.

Integral breadth of {111}, {200} and {222} diffractions was measured from each deposited film using Co–$K\alpha$ (40 kV, 0.1 A with graphite monochromator).

2.3. Determination of chemical composition rate of TiN–TiC films

It is not easy to determine the chemical composition of TiN–TiC mixed crystals by x-ray examination, because of the overlapping of the N–$K\alpha$ line (3.160 nm) with the Ti–$L\iota$ line (3.136 nm). In the present experiment the chemical composition of each sample was determined by statistical analysis and the curve fitting technique (Imada *et al* 1990) using EPMA operated at 15 kV and 50 μm in diameter. Figure 2(a) shows spectra obtained from the standard sample of TiN (dotted curve) and TiC (full curve), respectively, the former consists of Ti–$L\alpha$ (2.743 nm) and N–$K\alpha$ (3.160 nm) while the latter consists of Ti–$L\alpha$

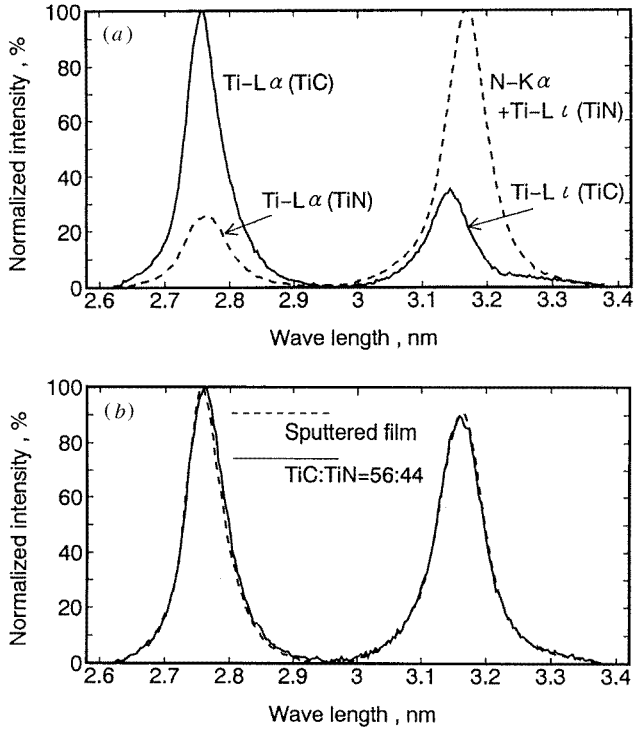

Figure 2. (a) Spectra obtained from TiN and TiC as standard samples from TiC and TiN. (b) Spectra obtained from a deposited film and from mixture of the standard samples (TiC:TiN = 56:44).

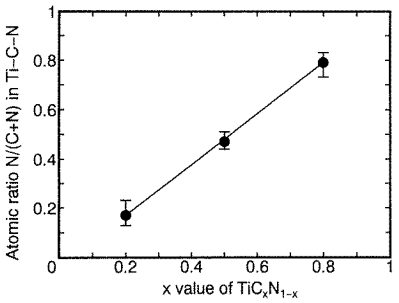

Figure 3. Relationship between the mixtures of TiC and TiN denoted by TiC_xN_{1-x} and their analytical results.

and Ti–$L\iota$ (3.136 nm). Figure 2(*b*) indicates the spectra obtained from the mixture of the standard samples TiN and TiC with 44% and 56% (dotted curve), and the spectra given by a film (full curve), respectively. It is seen that these two curves agree well. Therefore, the determination of the chemical composition of the film to be examined is quite sufficient to analyse them using our method (Imada *et al* 1990, 1992). TiN, TiC and TiNC powders of a special grade available in the market, 99% in purity and 2–5 μm in size, were used as the standard samples. Figure 3 illustrates the relationship between the mixture ratio of TiN to TiC and the analytical result in each film sample, indicating good agreement of the values.

2.4. Scratch and microhardness measurements

To evaluate the strength and adhesion of the deposited TiC–TiN mixed crystal film, Martens' scratch hardness (with a conical diamond of angle 90°, tip radius of 10 μm) was measured at load ranging from 3×10^{-2} to 1.4 N in vacuum. The scratching speed of 1 mm min^{-1} was used in this examination. The scratch width was obtained by measuring the average area per unit length for the scratch direction on each optical micrograph. The rupture of the coated film along the scratch direction was confirmed by an optical microscope in a region of the transition range (Nakanishi *et al* 1993). Microvickers' hardness test was carried out with coated samples at a load of 98.2 mN.

2.5. Friction and wear

Friction and wear experiments were carried out using a pin and plate type testing machine by reciprocal moving specimen (plate) against pin. The entire test machine was enveloped in a glass chamber to maintain test conditions during the examination. The overall design of the apparatus is illustrated in figure 4. The relative humidity of the chamber was put at 10%.

Wear of the film samples was measured using an analytical electronic balance (accuracy of 10 μg). The wear rate was determined as $w = W/1$, with 1 being the sliding distance and W the weight loss of film sample. The cycle rate of plate sample was taken to be 2 cycles/s with an alternating motion of amplitude, 18.2 mm, amplitude in the longitudinal direction passing the central point shown in figure 1. The nominal load on the interface was taken to be 1.2 N. Normally, the test was run for a 156 m sliding distance, and frictional force was monitored during the test. The friction coefficient of each sample was determined from the average frictional force measured at a portion corresponding to the middle of the scratch length.

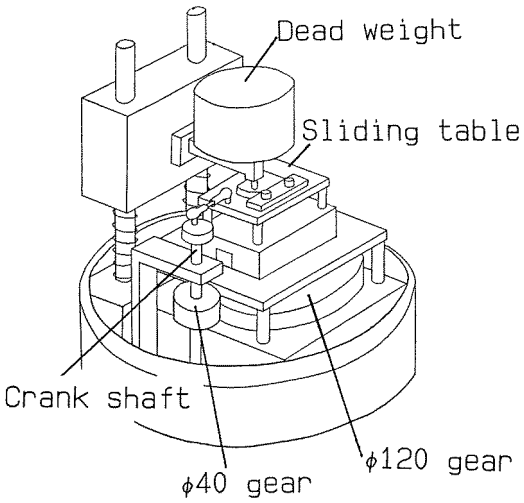

Figure 4. Schematic representation of friction and wear tester.

3. Experimental results

3.1. Chemical composition of deposited films and their thickness

The relationship between the substrate positions shown in figure 1 and the chemical composition of the film is shown in figure 5 as a function of the $N/(N + C)$ atom ratio. It is seen from this figure that: (1) continuous changes in composition were observed on deposited films according to the order of the substrate number, in which each data point ranging from $x = 0.2$ to 0.8 indicates the average concentration calculated from EPMA line analysis (the analysis was done in the lateral direction through the central point on each substrate); (2) the substrate position giving $x = 0.5$ clearly shifted towards the TiC side as shown in this figure. This was explained by the difference in sputter yield between TiN and TiC; the sputter rate is larger in TiN than in TiC. It was confirmed from the line analysis that the difference of the concentration ratio Δx between the mth substrate and the $(m + 1)$ or $(m - 1)$ substrate is within 0.06.

Film thickness and morphology of the samples thus prepared on each substrate were observed by SEM on the fracture sections. A plot of the film thickness (open circles) against the x-value is shown in figure 6. It is noted in this figure that the film thickness is in the range of 3.4 to 5.1 μm. Figure 7 is an example of the SEM result obtained from the sample corresponding to $x = 0.38$, showing a fibrous structure irrespective of the x-value. The growth morphology of TiN–TiC mixed crystal coatings under the present conditions may be considered to be nearly the same and conform to the 'zone-*T*' structure (Thornton 1977), which is characterized by a very fine fibrous microstructure.

3.2. Adhesion of film-to-substrate material

Figure 6 illustrates the adhesive force characterized by the critical load as a function of the x-value, showing a gradual increase with x and reaching maximum at about 0.5. The critical load for the onset of rupture of deposited film is generally defined as that load at which the film appeared to crack under optical microscopy. Bucher *et al* (1984) evaluated the adhesive force of TiN prepared by RF sputtering against a high-speed steel, and showed

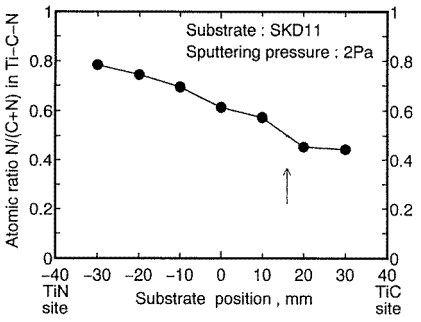

Figure 5. Variation of the x-value in TiC_xN_{1-x} with the substrate position.

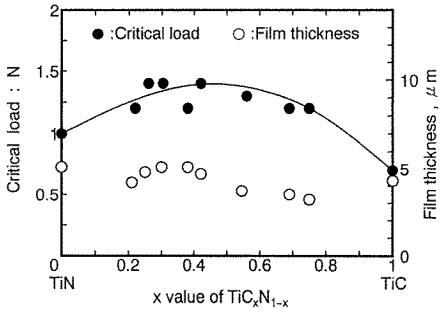

Figure 6. Variation of the critical load for the onset of fracture of deposited films as a function of the x-value. Open circles show the corresponding film thickness.

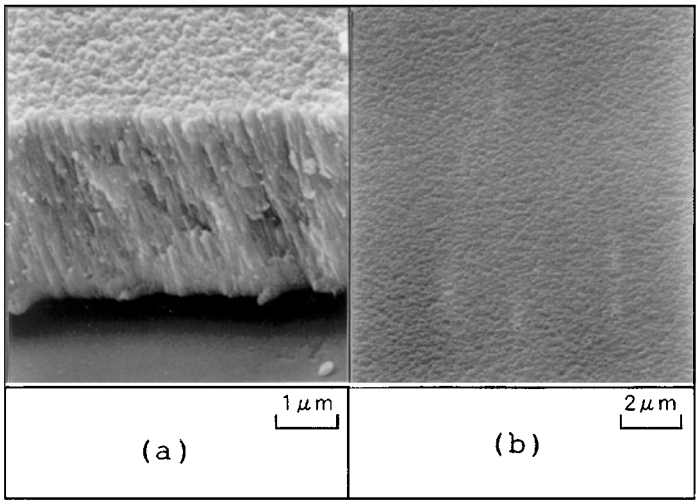

Figure 7. A typical scanning electron micrograph obtained from $TiC_{0.4}N_{0.6}$ (*a*) fracture section (*b*) specimen surface.

that the critical load reached maximum at about 4 μm, and did not result in further increase with increase of film thickness. Nakanishi *et al* (1993) studied the strength and adhesion of Al oxide film on steel and found that the relationship between the logarithmic scratch width and the logarithmic load in the coated samples is composed of one set of two straight lines differing in slope. A rupture of the film along the scratch direction was observed in the transition range from the two lines. The critical load m_0 corresponding to the transition in data appeared with increasing scratch load.

The force required to separate the interface, the adhesive force, is considered to be closely related to the interfacial energy; that is, the work is equal to the decrease in the free energy due to adhesion. Therefore, if C and N atoms in the TiN–TiC mixed crystal distribute randomly in their lattice points according to the carbon-to-nitrogen ratio, the adhesive force occurring on the interface between the crystal and substrate material must be altered monotonously as a function of the x-value. However, the obtained data were not the case as shown in figure 6, suggesting the existence of an ordered distribution in N and

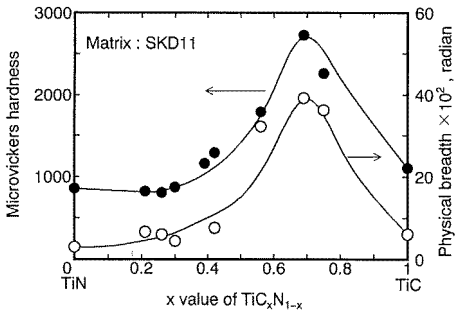

Figure 8. Variation of microhardness (closed circles) and of physical breadth obtained from {200} diffraction (open circles) with x-value.

C at about $x = 0.5$. Unfortunately, the distribution of N and C atoms in the matrix is very difficult because the atomic scattering factor in these two atoms is almost the same.

However, it is known that the adhesion test is very sensitive to the surface conditions such as asperity, oxide film, gas-adsorbed layer etc present on the surface. Yamamoto and Nakajima (1981) measured the adhesion force between two adhering bodies (needles and plates) for various materials using a stylus and plate. The method of the experiment used gives the adhesion force without reference to such surface conditions if the experiment was carried out with a stylus of a definite radius and a plate in high vacuum. Further study on the precise adhesion phenomenon without reference to any surface conditions is necessary.

3.3. Microhardness of film samples

Figure 8 shows the variation in the hardness of the deposited film with x-value. The concentration ratio has a large effect on the hardness; it became maximum at around 0.7, and reached at least 2750 kgf mm^{-2} (27 000 MP). A similar result relating to microhardness and tribological properties was reported by Bertoncello *et al* (1992), whose experiment on Ti(CN) film by reactive ion plating system showed the microhardness value to be significantly harder than those of TiC and TiN films, and also showed a lower friction coefficient and a higher level of wear resistance than those of TiN films. It should be noted here that the effect of substrate material on the hardness of deposited film increases as the film thickness decreases, and also the indentation load produces an effect on the microhardness. In fact, the hardness of TiN and TiC, as shown in this figure, is nearly half the ordinary value reported. It is possible, however, to recognise the present data as indicating a relative hardness across the whole sample with the average thickness of 4 μm. Figure 8 also shows variation in integral breadth with the x-value, showing that physical breadth corresponds well with that in the microhardness. Internal strain due to a high density of grain boundaries and lattice defects is considered to be an important factor in determining the hardness of polycrystalline film.

A number of papers have attempted to elucidate the influence of the preparation conditions on crystal orientation with TiN and TiC deposited films (Wang *et al* 1990, Uchiyama *et al* 1991). The mechanical properties of those films are superior in {200} oriented film to those in {111} oriented film. Figure 9 depicts the variation of microhardness with x-ray intensity ratio, $I(111)/I(200)$, as a function of the x-value, where $I(hkl)$ denotes the intensity of x-ray diffraction from the $\{hkl\}$ plane in the sample. The hardness indicates a rapid decrease at an initial stage, then gradually becoming constant at about 0.5 in

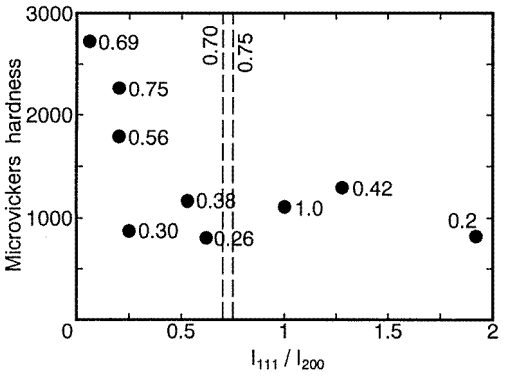

Figure 9. Microhardness plotted against $I(111)/I(200)$ value. Two dotted curves indicate the $I(100)/I(200)$ value given from the standard samples of TiN (0.7) and TiC (0.75), respectively. The superscript of each experimental point denotes the corresponding x-value.

$I(111)/I(200)$. The x-ray intensity ratio given from standard powder samples of TiN and TiC, which were denoted by dotted curves in this figure, correspond to 0.7 and 0.75, respectively; moreover the nominal value described in each experimental point indicates the x-value of the corresponding sample. It is seen from this figure that the microhardness decreased rapidly with increasing $I(111)/I(200)$ value. Another point to be noted in this figure is that the increase in hardness appears to be closely related to the degree of {200} preferred orientation, but not {111} preferred orientation.

3.4. Friction and wear

Figure 10(*a*) illustrates some examples of the variation in the friction coefficient with sliding distance. In this figure, the amount of scatter indicated by the difference between the maximum and minimum friction coefficient was about 10% or less in each sample. It can be seen from figure 10(*a*) that the behaviour of the friction coefficient–sliding distance curve seems to be essentially the same among the samples. For the first stage of sliding, the coefficient of friction rapidly decreases with sliding distance, after which it becomes constant. Figure 10(*b*) illustrates the variation in friction coefficient determined by the stable value in each curve with the x-value. It is seen from this figure that the friction coefficient decreased gradually and becomes almost constant at about $x = 0.4$.

A change in the specific wear rate is shown in figure 11. The result shows complex phenomena on the change in wear rate; it seems to have two regions showing maximum wear rate, a very large maximum at around 0.2 and a small one at about 0.8 in x-value. Electron probe micro-analysis confirmed that there are traces of Fe on the wear track, but shows a tendency to increase with increasing content of TiN. The result suggests that an affinity for Fe of TiN is larger than that of TiC. It is interesting to compare figure 9 with the data associated with the microhardness and preferred orientation in the samples. By comparing these two figures it may be said that the wear rate alters with the change in $I(111)/I(200)$ value; for instance, the maximum wear rate for TiC_xN_{x-1} ($x = 0.2$) corresponds fairly well with the minimum of microhardness and a high degree of {111} preferred orientation in sample.

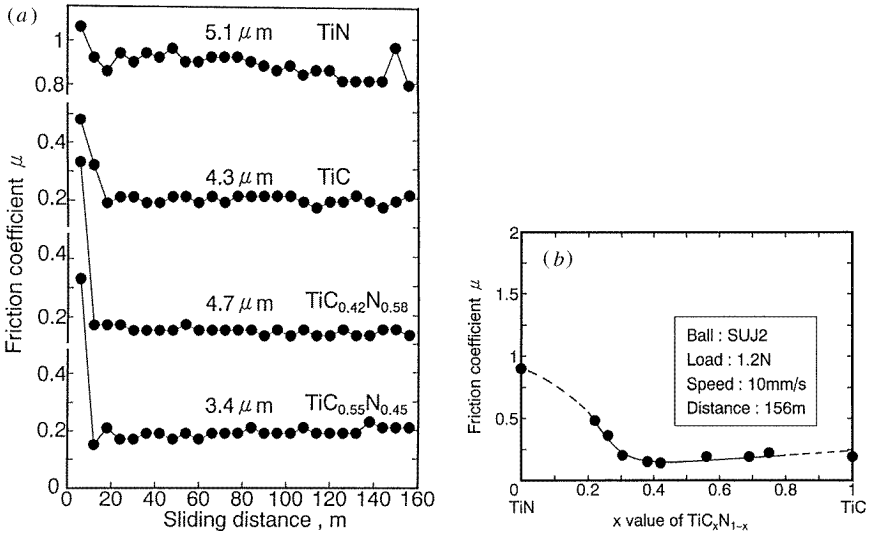

Figure 10. (*a*) Friction coefficient plotted against the sliding distance for TiC_xN_{1-x}. (*b*) Relationship between the friction coefficient and x-value in the TiN–TiC system.

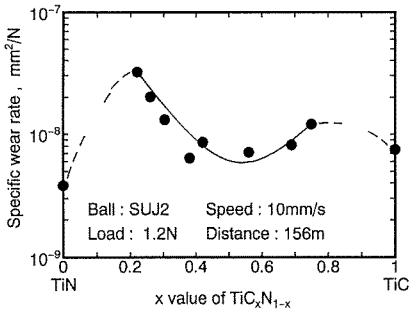

Figure 11. Variation in specific wear rate with the x-value for TiC_xN_{1-x}–SUJ2 couple.

4. Discussion

4.1. Effect of lattice strain and particle size on microhardness

In view of the evidence obtained that the physical breadth corresponded well to the change in the microhardness, an attempt can be made to evaluate the relation between the lattice strain or particle size and microhardness. The line-broadening analysis was then carried out with the data shown in figure 8 to estimate the effects of the strain and size on the hardness. The physical breadth, $\Delta 2\theta$ may be proportional to $1/\cos\theta$ (Schrrer formulae) in the case of the fragmentation of sub-structure, ε, and proportional to $\tan\theta$ in the case in which the broadening is of lattice strain, ξ. The following relation is given by diffractions of two orders, for example, {111} and {222}: $(\Delta 2\theta_{222}/\Delta 2\theta_{111})_\varepsilon$ denoted by $f(\varepsilon)$ is expressed in terms of $(\cos\theta_{222}/\cos_{111})_\varepsilon$ and $(\Delta 2\theta_{222}/\Delta 2\theta_{111})_\xi$ denoted by $f(\xi)$ is expressed in terms of $(\tan\theta_{111}/\tan\theta_{222})$.

$f(x)$, $(\Delta 2\theta_{222}/\Delta 2\theta_{111})_x$, measured from a given sample is considered to lie between the extreme of $f(\varepsilon)$ and $f(\xi)$. By using the following parameter D, it may be possible to

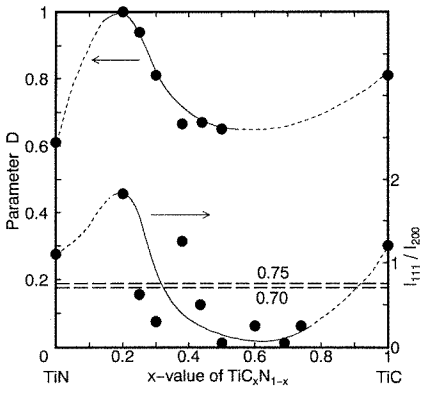

Figure 12. Parameter D and $I(111)/I(200)$ plotted against the x-value. The two dotted curves illustrated in this figure indicate the $I(111)/I(200)$ value obtained from TiC (0.75) and TiN (0.70), respectively, as standard samples.

Table 1. Peak shift between {111} and {200} diffractions and the calculated stacking fault probability of TiC_xN_{1-x}.

x	0	0.21	0.25	0.30	0.38	0.42	0.5	0.54	0.74	1.0
$\alpha \times 10^2$	1	1.5	2	2	3.5	4	3.5	...	...	2

$\Delta(2\theta_{111} - 2\theta_{200}) = 6.2\alpha$ for Co–$K\alpha$ radiation.

obtain information concerning the contribution of these factors to the observed broadening:

$$D = (f(\varepsilon) - f(x))/(f(\varepsilon) - f(\xi)).$$

The parameter D was characterized so that the value 0 may be given in the case of particle size and the value 1 in the case in which the observed line broadening is of lattice distortion.

Figure 12 represents a plot of D as a function of x-value; the parameter D displaces largely, but depending on x, towards a high value of more than 0.7 across the whole sample. This indicates that the major part of the line broadening shown in figure 8 is due to lattice distortion. Accordingly, the result suggests that the decrease in the amount of D-value below 0.5 leads to a further increase in the hardness. In fact, a reduction in grain size gives rise to high hardness (Sundgren 1985). It is also apparent that the situation in variation of D coincides markedly with that of the $I(111)/I(200)$ ratio; the increase of the {200} preferred orientation is associated to a certain degree with decrease of lattice distortion formed during deposition.

4.2. Generation of stacking faults in the film

It should be noted here that the peak position of {111} and {200} diffractions has shown the characteristic shift between them, indicating the existence of the stacking faults. The characteristic shift is defined as $(2\theta_{200}-2\theta_{111})_s-(2\theta_{200}-2\theta_{111})_d$. The first and second terms represent the angular differences between {111} and {200} obtained from one set of each sample, for example standard sample and the corresponding deposited film, respectively. It will be seen from table 1 that the stacking fault probability, α, increased with x and reached maximum at 0.4–0.5. However, the peak shift between the two displacements could not be measured due to the occurrence of strong {200} preferred orientation in the film, when the x-value increased the amount beyond around 0.6.

It is known that the stacking fault will be formed in the following case, if the single layer vacancy platelet lies on the {111} plane. In other words, the formation of stacking

faults suggests that such vacancy platelets corresponding to the stacking fault probability in density are produced in the film during the sputtering deposition. It is noted here that the dislocation mobility for nitrides is very low, below about 1000 °C.

5. Conclusion

The following conclusions were drawn from the above experimental results.

(1) By using a newly designed complex target, mixed crystals of TiN–TiC denoted by TiC_xN_{1-x} were prepared simultaneously in the x-value range of 0.2–0.8.

(2) The change in microhardness with the x-value coincided markedly with the change in integral breadth of {111} and {200} diffractions. It was shown from the parameter D that a major part of the line broadening was due to lattice distortion which occurred during the formation of the film.

(3) The decrease of the $I(111)/I(200)$ ratio was associated with the increase in microhardness.

(4) Adhesive force between the deposited film and substrate increased with x-value, and reached a maximum at about 0.5.

(5) This investigation showed that the low wear rate and low value of the friction coefficient can be obtained with x ranging from 0.4–0.6.

References

Bertoncello R, Casagrande A, Casarin M, Glisenti A, Lamzoni E, Mirenghi L and Tondello E 1992 TiN, TiC and Ti(CN) film characterization and its relationship to tribological behaviour *Surf. Interface Anal.* **18** 525–31

Bucher J P, Ackermann K P and Buschor F W 1984 R.F. reactively sputtered TiN: characterization and adhesion to materials of technical interest *Thin Solid Films* **122** 63–71

Imada Y, Honda F and Nakajima K 1990 Characterization of heterogeneous substances by EPMA *X-ray Anal.* **21** 111–21 (in Japanese)

Imada Y, Kamamura K, Honda F and Nakajima K 1992 The tribological reaction accompanying friction and wear of silicon nitride containing titanium nitride *ASME J. Tribology* **114** 230–5

Jamal T, Nimmagadda and Bunshah R F 1980 Friction and adhesive wear of titanium carbide and titanium nitride overlay coatings *Thin Solid Films* **73** 245–54

Nakanishi M, Okuyama H and Nakajima K 1993 Strength and adhesion of thin aluminium oxide film deposited on iron surface *ASME J. Tribology* **115** 615–19

Narasimhan K, Boppana S P and Bhat D G 1995 Development of a graded TiCN coating for cemented carbide cutting tools—a design approach *Wear* **188** 123–9

Ramalingam S and Winer W O 1980 Reactively sputtered TiN coatings for tribological applications *Thin Solid Films* **73** 267–74

Sundgren J E 1985 Structure and properties of TiN coatings *Thin Solid Films* **128** 21–44

Tamura M, Ando F, Nishida K, Iwasaki Y and Kodera T 1994 Wear properties of Ti–C–N coatings and their application to side trimmers *Surf. Technol.* **45** 619–24 (in Japanese)

Thornton J A 1977 High rate thick film growth *Ann. Rev. Mater. Sci.* **7** 239–60

Uchiyama Y, Hasaka M, Mori H and Matsutake H 1991 Orientation of TiN and TiC films coated by the PDV method *Surf. Technol.* **42** 1250–4 (in Japanese)

Wang D, Murata H and Oki T 1990 Orientation, morphology and properties of TiN films deposited by reactive ion plating *Surf. Technol.* **41** 382–7 (in Japanese)

Warren B E and Warekois E P 1955 Stacking fault in cold woked alpha–brass *Acta Metal.* **3** 473–9

Wittmer M 1985 Properties and microelectronic applications of thin films of refractory metal nitrides *J. Vac. Sci. Technol.* A **3** 1797–803

Yamamoto M and Nakajima K 1981 A study of the physical adhesive state between solids *Wear* **70** 321–7